Journal of Applied Fluid Mechanics, Vol. 17, No. 11, pp. 2313-2332, 2024.
Available online at www.jafmonline.net, ISSN 1735-3572, EISSN 1735-3645.
https://doi.org/10.47176/jafm.17.11.2686

Enhancing Bulb Turbine Performance Assessing Air Injection for Vibration Mitigation and Hydrofoil Cavitation

S. Praveen [1], S. Marimuthu [1†], B. Alqahtani [2], G. Bharathiraja [3] and G. Gokilakrishnan [4]

[1] *Department of Mechanical Engineering, Karpagam Academy of Higher Education, Coimbatore, India*
[2] *Mechanical engineering department, College of Engineering, Northern Border University, Arar 91431 Saudi Arabia*
[3] *Department of Mechanical Engineering, Saveetha School of Engineering, Saveetha Institute of Medical and Technical Sciences, Chennai, Tamil Nadu, 602105, India*
[4] *Department of Mechanical Engineering, Sri Eshwar College of Engineering, Coimbatore 641202, Tamil Nadu, India*

†*Corresponding Author Email: drsmarimuthu@gmail.com*

ABSTRACT

Small hydro technology is playing a crucial role in advancing sustainable, clean energy policies as part of the global hydro development strategy. Its contribution to social and economic development is becoming more prominent, particularly in ensuring electricity access for rural communities and supporting industrial expansion. The main causes of bulb turbine failures under high operating conditions are frequently attributed to variations in pressure in the draft tubes, which are aggravated when a spinning vortex rope is formed under load operation. Different fluid injection techniques, namely compressed air and water jet injection, address these issues and reduce the negative results of cavitation. The investigation covers the flow visualization on the suction side of a single hydrofoil utilizing a cavitation tunnel and a bulb turbine. This study assesses the effectiveness of compressed air injection in reducing vibration generated by cavitation in bulb turbines. Positive results of the experimental studies suggest a decrease in noise and vibration by air injection that prevents oscillations of the vortex rope. This research also considers how the hydrofoil design of bulb runner blades influences flow characteristics. Hence, it provides knowledge on cavitation structures in diverse cavitation numbers. Different studies that compare the original and modified hydrofoil designs reveal remarkable improvements that may be due to changes in the key parameters of the hydrofoil, such as later cavitation initiation and reduced intensity. To obtain the optimal output of a bulb turbine by considering air injection for vibration reduction and hydrofoil design changes to limit the negative effect of cavitation, the Reynolds number and cavitation number are to be defined. This multidisciplinary approach possesses enormous potential to increase the reliability and efficiency of bulb turbines in challenging operating conditions.

Article History

Received March 4, 2024
Revised May 21, 2024
Accepted May 27, 2024
Available online September 1, 2024

Keywords:

Hydropower
Bulb turbine
Rotating vortex rope
Compressed air injection
Part-load operation
Vibration
Cavitation

1. INTRODUCTION

The hydro turbine is a vital component in hydroelectric facilities' efficiency and operational aspects. Depending on the hydrological conditions of the site, Francis, Propeller, and Kaplan turbines are employed as either impulse or reaction turbines. Steady-state operation includes partial load, best efficiency point (BEP), full load, and overload, while transient operation involves start-stop, load variations, total load rejection, and shutdown Li et al. (2018). These pumps are also known as low-specific-speed pumps because they have lengthy and narrow impeller flow channels and a high fluid velocity at the pump intake (Zhu 2002; Jin et al., 2012). Consequently, cavitation is a real possibility in the flow, which may disrupt the internal flow pattern and drastically reduce the pump's efficiency.

Over the last several decades, researchers have focused heavily on cavitation in pumps. The renowned Rayleigh equation was proposed by Rayleigh (Lindsay 1970) using spherical symmetric cavitation as the study focus. Plesset and Prosperetti, (1966) took an essential step in the theory of cavitation dynamics. When they developed the Rayleigh Plesset equation. By considering the impacts of

NOMENCLATURE

d_{max}	amplitude of oscillation	φ	velocity potential
D	bulb turbine width	ϕ	flow number
s_{max}	maximum hydrofoil curvature	Q	volumetric flow
r_0	leading edge	Re	Reynolds number
σ	Thoma's cavitation factor	L	hydrofoil's length
N	rotating frequency	v	forward flow velocity
A_0	guide vane opening coefficient	p_{abs}	absolute pressure

gas, fluid viscosity, and surface tension, their study sought to enhance our comprehension of cavitation. Brennen et al. (1982) performed an extensive investigation to support this theoretical framework. Two cavitation inducers with the same geometry but different experimental dimensions were examined, and their dynamic transfer functions were compared. In order to better understand cavitation processes in fluid dynamics, this experimental study aimed to confirm and build upon the insights given by the Rayleigh-Plesset equation. Using four axisymmetric structures with their boundary layers separated luminary and then reattached turbulently, Cervone et al. (2009) investigated cavitation. Using holography and the Schlieren flow visualization method, we were able to identify the parameters for cavitation inception and design. Many holograms were also captured just before and at the commencement of cavitation. In an experimental investigation conducted by Tanaka and Tsukamoto (1999), the transient behavior of a cavitation centrifugal pump was examined. The researchers identified oscillating cavitation during pump start-up and the separation of the water column after an abrupt pump shutdown as the two primary factors responsible for changes in pressure and flow rate. In cavitation numerical simulation research, these findings provide a critical groundwork for theoretical comprehension and practical applications. In their study, four well-known models—the Kubota, Singhal, Merkle, and Kunz—were examined Huang et al. (2012). In order to evaluate the usefulness and effectiveness of different theoretical frameworks, this comparison is essential for moving cavitation research forward. In addition, (Al-Obaidi et al. 2023a; Cheng et al., 2021a). A thorough review of cavitation research advances offers essential background information and new perspectives on the field's present status, which may guide future research and methods design. This includes cavitation features, numerical approaches, cavitation's effect on the flow field, and certain frontier problems. In the last 20 years, researchers have increasingly turned to the Computational Fluid Dynamics (CFD) method to study fluid issues in pumps. Since the development and progression of cavitation are highly connected with the local turbulence, it is crucial to accurately estimate the pressure and fluid velocity in a pump and the turbulence (Al-Obaidi et al., 2023b; Cheng et al., 2021b). Selecting an appropriate turbulence model for pump flow modeling has been the subject of much research and development (Kral 1998; Wang et al., 2007; Nohmi et al., 2010; Sun et al., 2014; Al-Obaidi, 2023a) compared two approaches by simulating the internal flow of a pump-turbine system under varying operating circumstances using Computational Fluid Dynamics (CFD) methodologies. After comparing it to other two-equation models, the Detached Eddy Simulation (DES) model proved to be the most effective turbulence model. Results prove that DES is an excellent tool for forecasting the flow properties of hydraulic systems like these. Meanwhile, (Feng et al., 2010; Al-Obaidi, 2023b, 2024) simulated a centrifugal pump in both steady-state and transient situations, including both within and outside of the design. Their findings showed that the choice of the turbulence model unexpectedly had little effect on the pump head and energy efficiency prediction. Specifically, the average k-ε model was more accurate at forecasting fluid velocity, but the SST k-ὺ model was better at capturing turbulent features. Furthering this research, Zhou et al. (2012) employed both the SST k-ω model and the Spalart-Allmaras Detached Eddy Simulation (S-A DES) model to simulate a specific pump configuration. Both models could accurately predict pressure pulsations and power requirements across a range of flow rates, but the former model was marginally more effective. Using the Delayed Detached Eddy Simulation (DDES) model, Zhang et al. (2019) expanded the scope to low-speed centrifugal pumps and concentrated on the stalling effect. They were able to reproduce stalling-indicative transient flow behaviors and structures accurately in their models, including the jet wake close to the impeller blade outlet.

Moreover, in the realm of cavitation simulation for low-specific-speed pumps, Wang et al. (2019) introduced density correction to turbulence models such as the Re-Normalization Group (RNG) k-ε, SST k-ω, and Filter-based model (FBM). By bringing the experimental data and simulated predictions into closer alignment, these updated models deepened our comprehension of how these pump configurations handle cavitation. Finally, Limbach and Skoda (2017) studied the impact of surface roughness and operating parameters on pump performance. Insights into the intricate interplay of pump design, operating conditions, and turbulence modeling were advanced thanks to their meticulous analysis, which advanced the study of hydraulic machinery. Simulated cavitation flow in a low-specific-speed centrifugal pump using the commercial CFD program CFX.

In the non-cavitation stage, the simulation results were highly concordant with those of the related experiment. In addition, the low-Reynolds-number approaches allow for a more precise prediction of cavitation initiation at the diaphragm tongue. Focusing on the links between cavitation development and low-frequency vibrations ranging from 10~500Hz, Gao et al. (2017) examined the experimental and modeling findings of a low-specific-speed centrifugal pump's vibration characteristics and cavitation. Several studies have also investigated how the shape of the impeller affects the cavitation behavior of

low-specific-speed pumps. By substituting a mix of long and short blades, sometimes known as splitter blades, for the conventional impeller blade, cavitation may be successfully reduced Zhang et al. (2014).

Across a range of flow rates, Zhang et al. (2019) conducted a thorough quantitative analysis of the effects of short-blade curvature on pressure variations in a low-specific-speed centrifugal pump. According to their research, reducing the short blades' outlet angle to 12 degrees towards the pressure side significantly reduced the severity of turbulence and total pressure variation at the pump outlet. Because of this change, the streamlines within the flow channels are now better matched to the shape of the blade. Cavitation flow evolution in the flow channels of a low-specific-speed centrifugal pump and the influence of the intake attacking angle on impeller cavitation growth was investigated by Hu et al. (2020) using numerical simulations and hydraulic experiments. According to their findings, cavitation starts at the suction side of the blade's leading edge and quickly moves to the impeller's outlet as the cavitation number lowers. The blade's load near the tongue was found to be heavier than other blades, independent of cavitation. This highlights a significant element of the blade's performance under different situations. According to the literature review, two-equation turbulence models are often used to describe pump cavitation processes. This inclination probably originates from the fact that these models can predict when cavitation will start and how it will progress.

It should be noted that while more extensive eddy simulations (LES), Delayed Detached Eddy simulations (DDES), and detached eddy simulations (DES) need more computing power, they provide a more thorough understanding of pump flow topologies. It is also crucial to consider how the coolant differs from pure water in terms of material properties and temperature sensitivity while considering aeronautic cooling pumps. Understanding cavitation in these systems requires customized methodologies and specialized modelling techniques (Lin et al., 2022; Dönmez et al., 2023).

According to the various investigation results stated above, the reduction of vibration and cavitation of the flow in the bulb turbine are the major problems. Several techniques such as fluid injection, compressed and water jet injection are used to reduce the vibration and cavitation in the bulb turbine. This study presents a novel method for reducing vibration and mitigating cavitation in bulb turbine systems through the modification of turbine blade hydrofoil design. This research emphasizes the efficacy of a modified hydrofoil design in enhancing resistance against cavitation during prolonged high-flow conditions, as demonstrated through experimental analyses comparing two different hydrofoils. Visualization analyses conducted in a cavitation channel provide additional insights into the enhancements achieved through the modified hydrofoil design. Comparative analyses of modified and unmodified runner blades demonstrate a significant reduction in cavitation occurrence when modified hydrofoils are implemented, highlighting their effectiveness in addressing cavitation-related problems. The study establishes a correlation between the critical cavitation number (sc) and the turbine's specific speed (Ns) using model test reports. This correlation is important for determining operational boundaries and preventing cavitation. The effectiveness of the modified hydrofoil design in addressing cavitation-related challenges is confirmed through an air injection test, providing valuable insights for the development of more resilient and efficient turbine systems.

2. HYDROFOIL

Optimizing blade hydrofoils in bulb turbines is complex and aims to achieve many goals, including high power production, low vibration, improved strength, and less cavitation problems. Operators may increase service intervals, reduce welding and repair costs, and prevent financial losses from nonoperational downtime by reducing cavitation. This investigation focuses on a particular range of volumetric flows that occur at a 25-degree angle to the blade—a configuration in which cavitation often occurs at flows that are 15% greater than the maximum efficiency point. Turbine manufacturers and consumers usually choose a 25-degree blade angle because it is consistent with standard operating circumstances and shows a higher risk of cavitation. The hydrofoil formed by the bulb runner blades is crucial in determining the turbine's flow characteristics. Effectively engineered three-dimensional blade hydrofoils play a vital role in reducing the onset and spread of cavitation on the runner's surfaces. Multiple hydrofoils are usually used to characterize the turbine runner blade correctly. Their combined profiles are then utilized to produce a smooth 3D geometry for further computational fluid dynamics (CFD) or experimental research, as shown in Fig. 1.

Despite the possibility that a bulb turbine blade may have many hydrofoils, we restrict our emphasis in this work to only one. The choice to focus on a single hydrofoil is based on the understanding that the area close to the bulb turbines' tip has the most energy conversion potential. This region is subject to increased tangential blade velocity and flow velocities, which create notable pressure gradients and put it near the tip gap flow, making it vulnerable to surface erosion and cavitation. In this area,

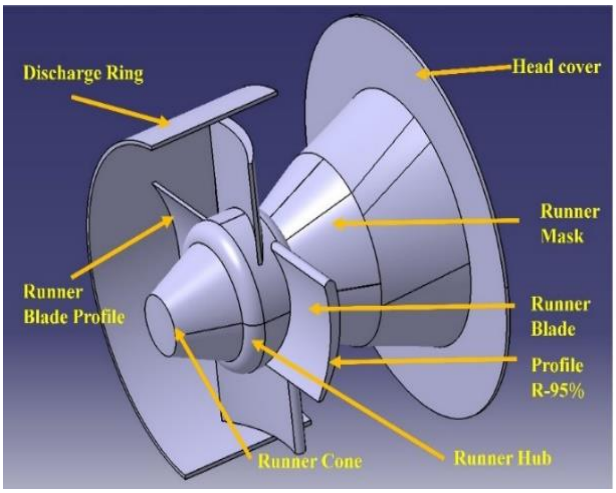

Fig. 1 Representation diagram of Bulb turbine runner

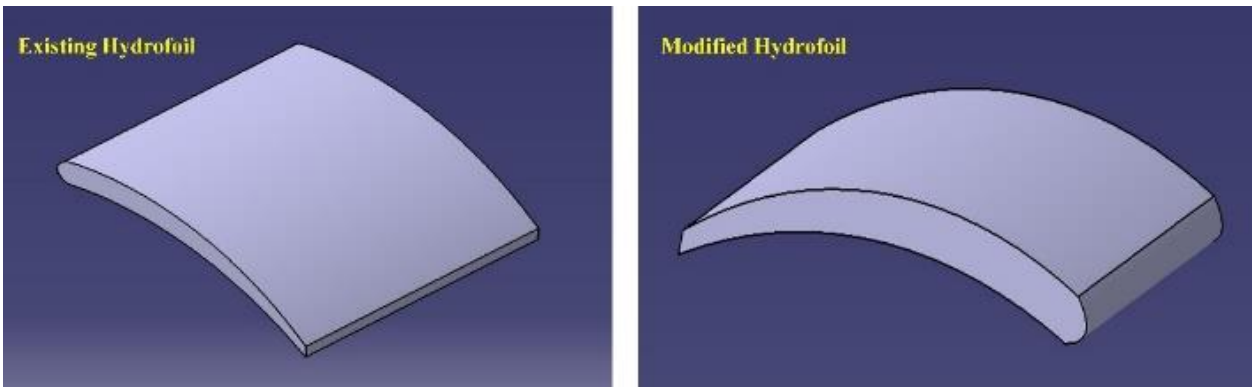

Fig. 2 Cavitation analysis Existing and Modified Hydrofoil

Table1. Features of hydrofoils.

Consideration	Changed	Unchanged
RunnerdiameterD_0	ø350mm	ø350mm
Number of runner blades Z	4	4
Ratiol_2/l	30%	45%
Maximumcurvaturel_2	54.2mm	81.3mm
Ratiol_1/l	15%	40%
Maximumthicknessl_1	27.11 mm	72.28 mm
Length of Bladechordlineat95%R	180.7 mm	180.7 mm
Angle of bladeβ_0	25°	25°
Hydrofoil references R_h	95%D_0	95%D_0
Radius of leading edge r_0	1.63mm	1.27mm

many cavitation structures usually appear during acceptance testing. We specifically opted for the hydrofoil positioned at 95% of the bulb turbine width (D), as measured from the runner revolution axis to the blade tip, to investigate the cavitation characteristics of the hydrofoils further. This strategic decision places the selected hydrofoil at the tip, where energy transmission is most prominent. The rationale behind this choice is rooted in the understanding that areas with larger blade diameters, extensive surface area, and high blade and flow velocities are optimal for energy transmission. This focused approach facilitates a comprehensive analysis of the cavitation phenomena in a critical section of the bulb turbine blade, offering valuable insights into the blade's durability and performance. Hydrofoil profiles such as NACA (notably the 4-8 series), Göttingen, Munk, NPL, and others have been extensively researched.

Regarding high volumetric flows, runner blade angles, and various operating conditions, turbine engineers have numerous options for choosing hydrofoils from these profile families. To minimize cavitation and maximize performance, turbine designers meticulously consider crucial hydrofoil characteristics such as leading-edge radius, camber, maximum curvature, placement of maximum thickness, and trailing edge design. It is widely acknowledged that bulb turbine blades are prone to experiencing cavitation, especially in the high discharge area. This phenomenon typically manifests on the blade's suction side, pressure side, fillet, and tip gap. The leading edge radius, maximum thickness position, and curvature are hydrofoil characteristics that significantly affect the suction and pressure side cavitation tendencies. Making sure the leading edge is smooth is usually the primary goal when designing to avoid cavitation and flow separation. Flow characteristics become more noticeable with a higher blade velocity at 95% of the blade radius, which might cause flow separation and impact cavitation characteristics. We postulate that, despite the complexity of flow dynamics, there is a link between bulb runner cavitation and the cavitation behavior of bulb turbine blades based on the cavitation analysis of a single hydrofoil in a water tunnel. The intricate flow dynamics inside a bulb turbine could make it such that the pressure distribution and flow characteristics near certain hydrofoils in a cavitation tunnel don't accurately portray the circumstances around the blades.

2.1 Hydrofoil Modification

The essential components of turbine blades are hydrofoils. Improving efficiency calls for a comprehensive 3D redesign of the bulb turbine runner blade, emphasizing uniformly and smoothly reshaping the turbine hydrofoil profiles. The modern blade has a larger leading-edge radius, a forward-shifted maximum thickness, and a forward-shifted maximum hydrofoil curvature than its predecessor. You can find all the information about the two turbine hydrofoils in Table 1.

Figure 2. Illustrates the existing and modified hydrofoil. The length of the hydrofoil chord in the modified version is 60 mm, the same as in the original. However, changes in a number of factors are apparent. The redesigned design features a slightly higher maximum hydrofoil thickness (d_{max}) of 2.55 mm compared to the old hydrofoil. The maximum thickness location (l_1) has also decreased from 24 mm to 9 mm, indicating a forward displacement. The maximum thickness position ratio (l_1/l), which was 40% before the change, is now 15% after the adjustment. Likewise, at 0.87 mm, the improved design's maximum hydrofoil curvature (S_{max}) is identical to the old hydrofoils. The maximum curvature location (l2) is now 18 mm ahead of where it was 27 mm before. So, the maximum curvature position ratio (l2/l) is now 30% instead of 45%. In addition, the updated hydrofoil now has a radius of 0.54 mm at the leading edge (r_0), up from 0.42 mm in the original hydrofoil. These adjustments aim to make the hydrofoils used in turbine blades more efficient and effective.

2.2. Identification of Cavitation

The physical occurrence of air bubbles forming and collapsing inside the flow area of a turbine is known as cavitation. Its prediction must define pressure and velocity distributions, particularly in regions where cavitation is expected to occur. Cavitation is most likely to happen in the runner and draught tube. The critical statistic to measure cavitation in hydraulic turbines is Thoma's cavitation factor (σ). This is reliant on the configuration, construction, and real-world performance of the hydraulic turbines. Cavitation, which disturbs flow and harms turbine parts, is a multiphase, three-dimensional, irregular occurrence. Cavitation can have unforeseen consequences for hydraulic machinery, including flow instability, excessive vibration, material surface degradation, and lower machine performance. Unreasonably, as cavitation intensity increases, these issues are becoming more problematic. Reduced size is the first and most important criterion for boosting a turbine's output power because it lowers the cost of its parts. As a result, the speeds are enhanced, and the cavitation number is minimized.

The bulb turbine is anticipated to suffer cavitation in numerous regions, which include the tip clearance, the runner blade's suction side, and the blade tip. A different type of cavitation related to tip clearance is tip vortex cavitation. Tip vortex cavitation is a unique form of tip clearance-related cavitation. The tip vortex occurs around the blade's leading edge, splits on the suction side, and then proceeds downstream to lower the runner blade. The effective design of the anti-cavitation lip may lower it. Determining the dimension and power of the tip vortex makes it easy to build the anti-cavitation lips accurately.

3. EXPERIMENTAL SETUPS

Physical models are tested in reputable laboratories, or prototypes are tested on-site as part of the experimental approaches to forecast cavitation. Experimental model testing can reduce or remove the cavitation, vibration, pressure pulsation, and hydraulic thrust issues. The universal norm for testing hydraulic turbine units is IEC 60193. IEC-60193 is extensively utilized for designating any form of reaction or impulse turbine that has been examined in a particular set of laboratory contexts; consequently, it can also be applied to the acceptance testing of prototype turbines. The position of the cavity inside the hydraulic turbine and its dynamics are used to forecast cavitation. Measurements and flow visualization in lab equipment, including a high-velocity cavitation tunnel and testing of models, were utilized to collect such information. To anticipate cavitation in the experimental approach, sensors are positioned at multiple places to observe a wide range of variables, including the level of the upper reservoir, which includes flow rates, changing pressure, consumption and exit stress, structural vibration, torque, and power. The turbine may function without cavitation under ideal working circumstances; however, on the site, it usually operates in less ideal settings. The distribution of pressure and velocity may have been impacted, which could cause the cavitation issue. While cavitation in the turbine cannot be prevented, numerous researchers have developed remedial strategies to lessen its effects on hydro turbine performance and maintenance. Managing pressure discharge in the turbine space is a crucial prerequisite for most cavitation mitigation systems. By determining the source of erosion, the process of erosion, and prevention techniques such as compressed air injection, which are described below, it is possible to reduce the likelihood that turbine components will fail due to cavitation erosion and surface fatigue. The air injection mechanism is a crucial safeguard against cavitation while the turbine operates. Utilizing the turbine under partial, complete, or overload loads increases the cavitation fluid flow's dynamic instability, resulting in power and pressure oscillations. One of the practical methods to reduce these pulsations is to add compressed air to the flow. The injection of compressed air underneath the runner while the turbine is operating can frequently greatly lower the magnitude of such pulsations. This method's discharge ring drives pressured air into the runner's centerline's horizontal plane. The airflow is injected across all tubes into each injection site at a consistent pressure and discharge. The introduction of air into the hydraulic turbines in different areas resulted in a nearly two-fold reduction in the rate of pressure pulsations. The air injection approach was applied to the bulb turbine model to minimize cavitation and lower vibration. The stainless-steel manifold is evenly drilled with holes of the same diameter. Compressed air was injected slightly higher than the runner blade's centerline to lessen discharge ring cavitation and tip vortex damage. Noise, vibration, and erosion may result from vortex cavitation leaks at the tip of axial flow turbines. The air injection has led to a reduction in cavitation damage and cavitation tip leakage. A methodology has been created to determine how tip-leaking cavitation and guide vanes interact. The air injection lowers the vibration level of the turbine parts and diminishes tip-flowing cavitation's potential for erosive damage. As water flows towards a region containing a pressure lower than the vapor pressure at this temperature, it begins boiling and generates quite a few tiny bubbles or cavities. The difference between air and vapor pressure determines where cavities will develop. Cavitation occurs in this case study near the discharge ring of the bulb turbines. Cavitation noise and vibration are its most noticeable side effects. Experimental research has revealed that a significant amount of noise is created when cavities collapse. The cavitation process generates significant fluctuating forces. Vibration arises when the inherent frequency of the machine shaft coincides with the frequency components of these variations. Cavitation creates vibration in a bulb turbine, and the frequency of the vibration, 1120 Hz, is relatively high.

3.1. Measurements of Turbine

A specific measurement station was set up at the Kolektor Turboinštitut in Ljubljana, Slovenia, to assess the efficiency of low-head axial and bulb turbines, as shown in Fig. 3. Consistency and dependability were ensured throughout model, witness, and acceptance testing by Zhang et al. (2022) by meticulously adhering to established processes during the development of this measuring station. Following standard protocols, we automated all measurement and data-gathering operations to ensure accuracy. The nominal runner diameter of the

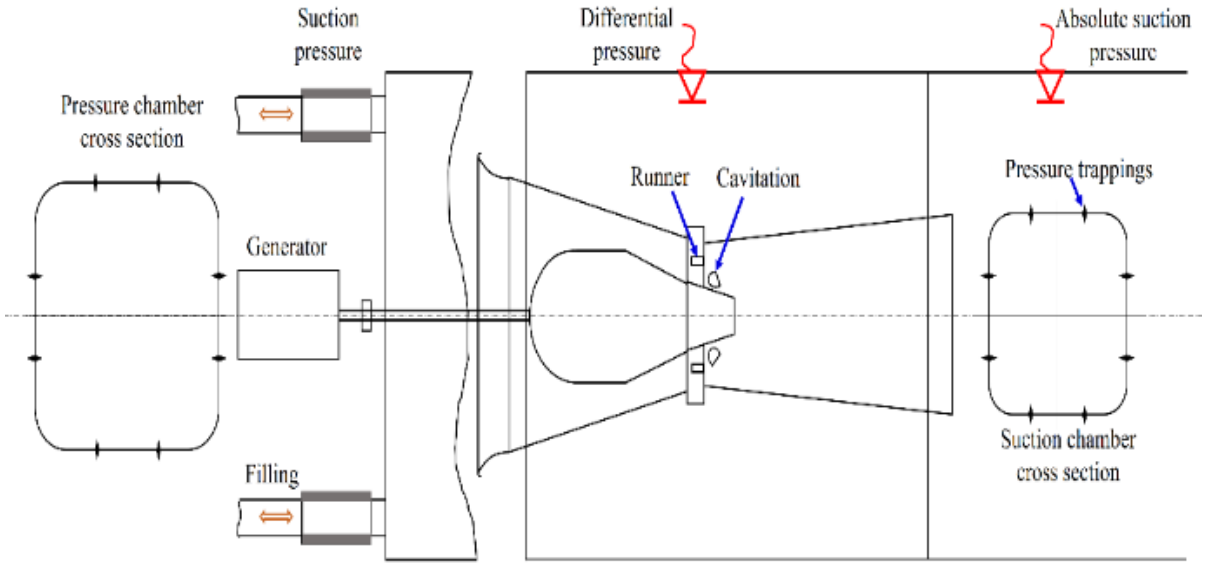

Fig. 3 Cavitation Measuring Station in Turbine

testing equipment is 350 mm, and it uses two frequency-adjustable radial pumps to provide recirculating flow. The electromagnetic flow meter enables the measurement of flow rate with an accuracy level of ±0.15% and a diameter of DN 400. With an accuracy of ±0.025%, differential pressure transducers may measure static pressure at both the input and outflow points. An absolute pressure transducer that measures total suction pressure to within ±0.025% precision is used to ensure activities are done at levels considerably above the incipient cavitation number. In addition, a counter-timer module processes the output from an electromagnetic incremental sensor, which measures rotational speed to within ±0.01% precision Al-Obaidi and Alhamid (2023). To accurately evaluate the performance and efficiency of turbines, these exact measuring processes and instruments are required. A horizontal shaft was used to measure shaft torque using a spinning torque transducer, and the accuracy was found to be within ±0.01%. By using air, we were able to estimate the friction torque. These thorough monitoring methods and data achieved an accurate assessment of turbine performance.

In order to compare, both runners were functioning at the identical specific energy E (J/kg), and the corresponding non dimensional energy numbers ψ were noted. The specific energy E was derived from the total specific energy at the turbine inlet and outlet cross-sections. The energy numbers ψ were computed using the specified equation.

$$\psi = \frac{2 \times E}{\Pi^2 \times N^2 \times D^2} \quad \text{.....} \quad (1)$$

The rotating frequency, N, is given in revolutions per minute (min^{-1}), and the discharge ring diameter, D, is shown in meters (m) for the bulb turbine. The turbine's rotational frequency, N ($1000min^{-1}$), was always the same Candel et al. (2014). Furthermore, the two runners' nominal diameters, D (m), were equal. Every set of comparison measurements showed that the guide vane opening coefficient, A_0, was constant.

$$A_0 = \frac{a_v \times z}{D_v} \quad \text{.....} \quad (2)$$

The number of guide vanes is represented by "z" and the opening of the guide vane is represented by "a_v" in millimeters (mm). Another thing that "D_v" stands for is the millimeter value for the guiding vane pivot diameter. Consistency in critical production processes and attributes allowed a trustworthy comparison of the two runners. Precise control over the clearances between the guide vanes and the pressure rings of the guide vanes and the gaps between the runners and the discharge ring is essential for reliable estimation of the runners in a model turbine. The materials and manufacturing processes used to make the two runners were similar. Hence, both runners were standardized concerning surface finishes, guide vane clearances, and tip gaps Grist (2023). A closed system was the mode of operation of the measurement station. To keep a constant "ϕ" the primary water circulation pump's frequency was controlled. The flow number "ϕ" is the non-dimensional representation of the volumetric flow, which is denoted as "Q" in cubic meters per second (m^3/s) Celebioglu et al. (2017)

$$\phi = \frac{Q}{\pi^2/4 \times N \times D^3} \quad \text{.....} \quad (3)$$

An earlier study found that using the same runner shape improved efficiency by around 1%. This improvement is mainly due to a change in operating points towards lower flow numbers and greater efficiency, as seen in the hill diagram analysis Al-Obaidi (2019). Figure 4. Illustrates measuring points of the turbine based on original hydrofoil, modified hydrofoil, and angled about 250 based on flow and energy rate numbers. These numbers are found by using Equation 1, 2, 3.

3.2. Measurements of Cavitation Tunnel

A closed-type cavitation measuring station, as shown in Fig. 5, was used for the flow visualization measurements. This arrangement is quite similar to an earlier experiment to study the flow properties of turbine blades in a dedicated

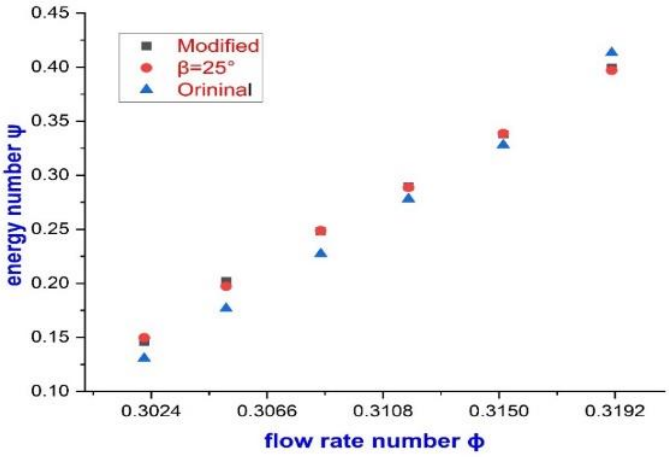

Fig. 4 Measuring point of Turbine

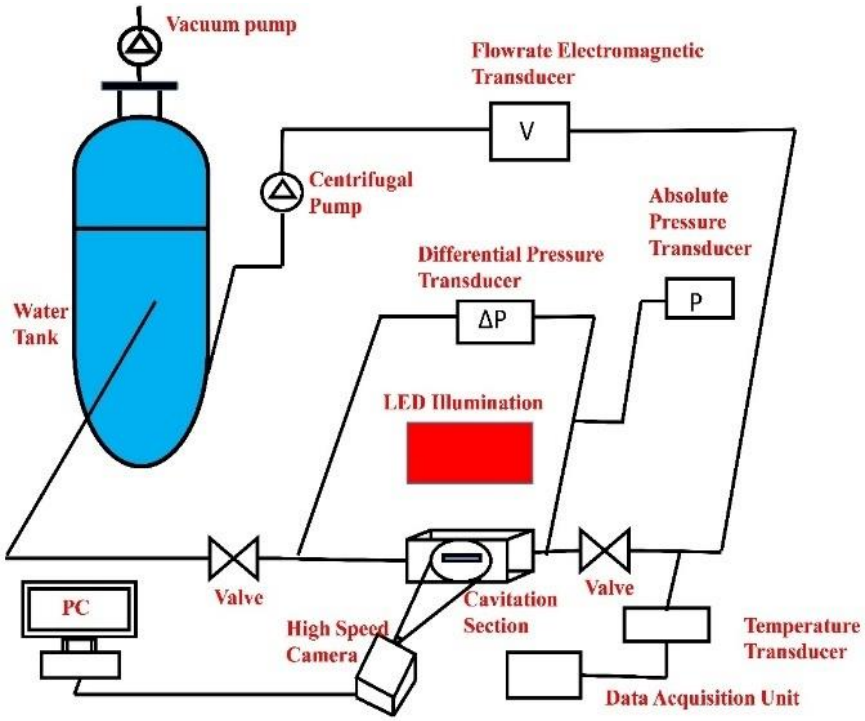

Fig. 5 Cavitation Measurement with Visualization Equipment

tunnel. A frequency-variable driving system powered a centrifugal pump, which supplied the flow. An ABB 2600T 264NS pressure transducer was used to measure the absolute pressure on the suction side. An ABB COPA-XL electromagnetic transducer was used to calculate the volumetric flow. A Pt-100 4-wire temperature transducer was connected to an Agilent 34970A data-collecting system to get temperature readings. Except for the setup procedures, most of the valves were left open throughout the experiment. Situated atop a tank with an exposed water surface, a vacuum pump controlled the suction pressure. The effects of cavitation on flow dynamics may be accurately assessed under these well-regulated circumstances, thanks to the rigorous setup.

The cavitation number (σ) and the Reynolds number (Re) are two dimensionless quantities we have chosen to describe cavitation in the cavitation tunnel.

$$Re = \frac{L \times V}{v} \quad \text{.....} \tag{4}$$

Cavitation numbers (σ) were calculated to evaluate the hydrofoil's cavitation properties. The hydrofoil's length (L), the forward flow velocity (V) in m/s, and the water's kinematic viscosity (v) were the three factors used to calculate these.

$$\sigma = \frac{P_{abs} - P_v}{\rho \times V^2} \quad \text{.....} \tag{5}$$

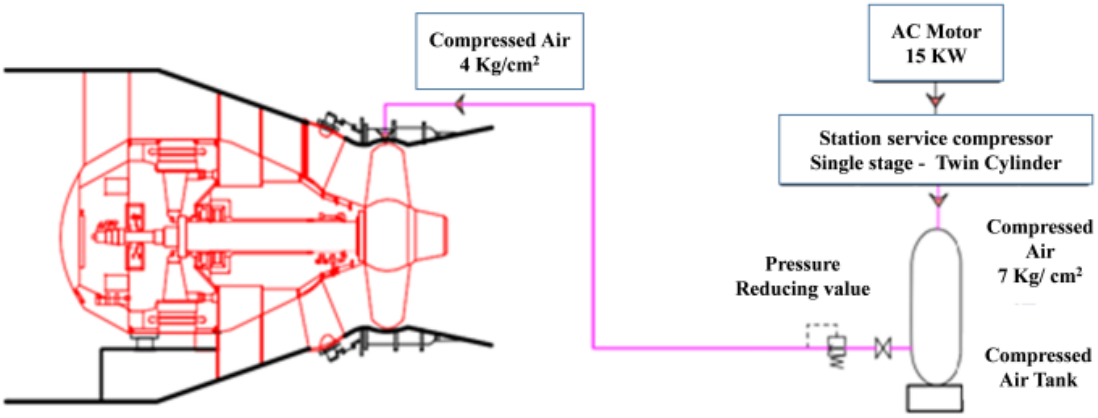

Fig. 6 Layout for air injection test

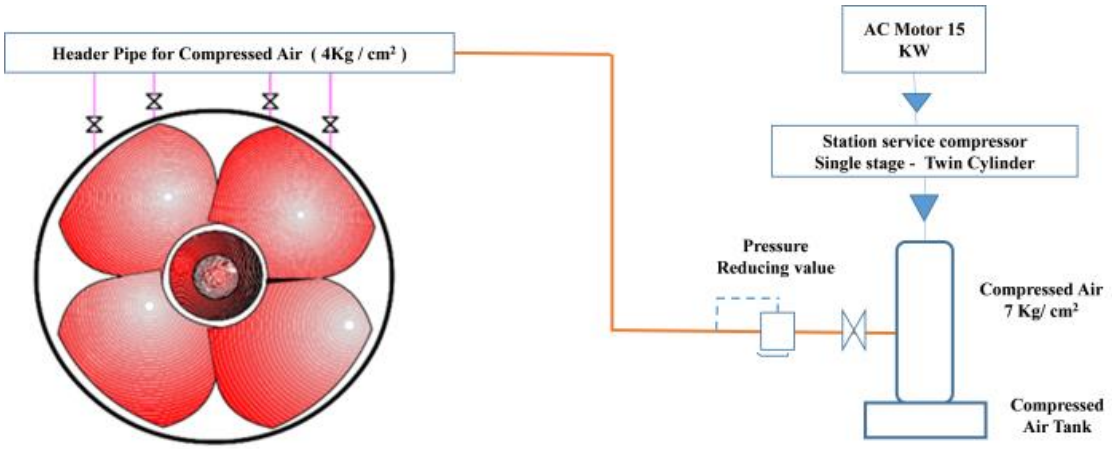

Fig. 7 Setup for an air injection test experiment

The most critical factors in the computations were the absolute pressure (P_{abs}) and the water evaporation pressure (P_v). We used the above equation to approximate the water evaporation pressure Cherny et al. (2010).

$$P_v = 10^{2.7862+0.0312.T_w-0.000104.T_w^2} \quad \text{.....} \quad \text{.....} \quad (6)$$

Where $T_w$is the temperature of the water in degrees Celsius (°C), as shown in Equation (6). The impact on the measurements is deemed insignificant since this Equation guarantees a maximum difference of 0.2%.

4. RESULTS AND DISCUSSION

To assess performance and ascertain whether vibration and noise levels have decreased, research on air injection has been conducted in bulb turbines. Four sets of copper pipes at 4 bar constant pressure with a 20 mm diameter that was designed to carry water for condenser runner vane cooling are employed for air injection into the turbine. The dummy flange was opened from the head to test the amount of air needed inside the discharge ring during operation, and it was discovered that water flowed easily at 30% guide vane openness. However, the unhindered water flow abruptly stops when the guiding vane openness rises from 30% to 34%. Additionally, there is also an acoustic bell-ringing sound and vibration. It is demonstrated that as soon as cavitation begins, a vacuum begins to form inside the discharge ring, along with vibration and noise. The low-pressure areas were given access to compressed air, which softened cavity collapses and lessened their damaging impact. The introduction of air breaks the vacuum in certain areas, increases the pressure, and eradicates the cavitation. The massive volume of air acts as a cushion, preventing the gigantic bubbles produced by the air pumped in this manner from collapsing while being crushed downstream in the high-pressure area. The air injection into the bulb turbine's runner vane moving area, as depicted in Figs 6 and 7.

4.1. Measurements of the Noise and Vibration Levels Made Vertically Beginning at the Discharge Ring's Top

Table 2 displays the noise and vertical vibration readings obtained from the peak of the discharge ring. While the plant is running and supplying 2 MW to the grid, the vibration is 77 μ, and when the machine is shut down while providing 2 MW to the grid. The noise level is 105 dB at the guide vane opening of 32% and runner vane opening at 2% during regular operation without air injection, whereas the vibration and noise levels are 73 μ and 100 dB, respectively. During regular operation without air injection, the machine that was producing 5 MW for the grid was shut off at guide vane openness (41%) and runner vane opening (19%) Dhinakarraj et al. (2020).

When the machine shuts down and sends 2 MW to the grid, there is an apparent level of vibration and noise while the guide vane opens narrowly at 32% and the runner vane opens narrowly at 2%. When the machine generating 5 MW for the grid is turned off, the guide vane is wide open

Table 2 Measurements of the noise and vibration levels were made vertically at the top of the discharge ring

Description of tests	Metrics obtained	Without air injection	With air injection	Guide vane/runner vane position
As of the starting point	Vibration (μ)	23	10	Guide vane opening time from 0% to 19% = 8 sec Guide vane opening time from 9 to 6 % = 9 sec Runner vane opening time from 100 to 0% =20 sec Guide vane opening =5 % Runner vane opening = 0 %
	Noise Level dB	95	87	
When a machine turns mechanically just before it shuts down	Vibration (μ)	71	51	Guide vane opening =5 % Runner vane opening= 0 %
	Noise Level dB	103	81	
During shutdown, when there is no load on the machine's grid.	Vibration (μ)	75	54	Guide vane opening =19 % Runner vane opening =0 % Guide vane the end interval from 19 to 0%= 1 sec Runner vane timing of opening from 0 to 100 % = 21 sec
	Noise Level dB	106	84	
The machine was delivering 2MW to the grid at the moment of shutdown.	Vibration (μ)	77	59	Guide vane opening = 32% Runner vane opening =2% Guide vane closing time from 32 to 19 % = 4 sec Guide vane closing time from 19 to 0 % = 1.5 sec Runner vane closing time from 2 to 0 % = 1.5 sec Runner vane opening time from 0 to 100 % = 21 sec
	Noise Level dB	105	91	
When the device that was supplying 5 MW to the grid was turned off	Vibration (μ)	73	55	Guide vane opening = 41% Runner vane opening =9% Guide vane closing time from 41to19 % =5 sec Guide vane closing time from 19 to 0 % = 1.5 sec Runner vane closing time from 19 to 0 % = 5.5 sec Runner vane opening time from 0 to 100 % = 23 sec

at 41%, and the runner vane is wide open at 19%, which results in relatively low vibration and noise levels, which are the design parameters of the machine. Hence, the vibration and noise levels are low when the machine delivers 5 MW compared to 2 MW due to the wide opening of the water passage Candel et al. (2014). It is to be noted that the machine supplier is not recommending operating the machine at 2 MW continuously to reduce the vibration and increase the life of the entire machine. It is seen from Table 1 that the vibration and noise levels were significantly reduced to 59 μ and 91 dB, respectively, during shutdown when the machine was using 2 MW of air injection. Similarly, the vibration and noise levels were significantly reduced to 55 μ and 86 dB, respectively. The machine was running at 5 MW with air injection at the shutdown time.

4.2. Measurements of Noise and Vibration in a Horizontal Direction on the Turbine Guide Bearing

The measurements of noise level and horizontal vibration on the turbine guide bearing are displayed in Table 3. During typical operation without air injection, when the system transmits 2 MW to the grid at the guide vane opening 32% and the runner vane opening 2%, the vibration level is 245, and the noise level is 121 dB at shutdown; in contrast, the vibration and noise level are 202 and 103 dB at shutdown when the machine is delivering 5 MW to the grid at the guide vane opening 41%. The runner vane opening 19% during regular operation without air injection. Due to the guide vane's small opening at 32% and the runner vane's 2% opening, there is relatively significant vibration and noise during the machine's shutdown when it produces 2 MW to the grid. The machine's design features, a large guide vane aperture of 41% and a big runner vane aperture of 19%, result in relatively low vibration and noise levels during shutdown while the machine supplies 5 MW to the grid. Hence, the vibration and noise levels are low when the machine delivers 5 MW compared to 2 MW due to the wide opening of the water passage. It is to be noted that the machine supplier is not recommending operating the

Table 3 Measurements of noise and vibration on the turbine guide bearing in a horizontal direction

Description of tests	Parameters measured	Without air injection	With air injection	Guide vane/runner vane position
As of the starting point	Vibration (μ)	66	43	Guider vane opening time from 0 to 19 % = 8 sec Guider vane opening time from 19 to 6 % = 9 sec Runner vane opening time from 100 to 0 % =20sec Guider vane opening = 5 % Runner vane opening = 0 %
	Noise Level dB	96	84	
when a machine turns mechanically just before it shuts down	Vibration (μ)	101	79	Guider vane opening = 5 % Runner vane opening = 0 %
	Noise Level dB	101	79	
During shutdown, when there is no load on the machine's grid.	Vibration (μ)	152	119	Guider vane opening = 19% Runner vane opening = 0% Guider vane closing time from 19 to 0 % = 1 sec Runner vane opening time from 0 to 100 % = 21sec
	Noise Level dB	106	84	
The machine was delivering 2MW to the grid at the moment of shutdown.	Vibration (μ)	245	168	Guider vane opening = 32% Runner vane opening = 2% Guider vane closing time from 32 to 19 % = 4 sec Guider vane closing time from 19 to 0 % = 1.5 sec Runner vane closing time from 2 to 0 % = 1.5sec Runner vane opening time from 0 to 100 % = 21 sec
	Noise Level dB	121	99	
When the device that was supplying 5 MW to the grid was turned off	Vibration (μ)	202	149	Guider vane opening = 41% Runner vane opening = 19% Guider vane closing time from 41 to 19 % = 5 sec Guider vane closing time from 19 to 0 % = 1.5 sec Runner vane closing time from 19 to 0 % = 5.5sec Runner vane opening time from 0 to 100 % = 23 sec

machine at 2 MW continuously to reduce the vibration and increase the life of the entire machine.

Table 3 illustrates that when the machine operates at 2 MW with air injection, the vibration and noise levels are dramatically reduced to 168 and 99 dB, respectively. When the machine shuts down while operating at 5 MW with air injection, the vibration and noise levels are significantly reduced to 149 and 84 dB, respectively.

4.3. Vertical Vibration Measurements on the Discharge Ring's Top

In continuous trials, a very small amount of injected air on the order of 1% by volume could be achieved. Nevertheless, it has a significant impact on the dynamics of cavitation. To more accurately characterize the change from pure cavitation to aerated cavitation, reducing the amount of injected air would be exciting. These findings will also serve as a reference point for developing numerical models of aerated cavitation. Figure 8 compares how the discharge ring vibrates vertically during an air injection test.

During air injection, a sharp reduction in vibration intensity is observed for discharges between 45 m^3/s and 125 m^3/s. Due to the pressurized air injected circumferentially at four equal locations to eliminate the vacuum created inside the discharge ring, a smooth flow of water is attained without any vacuum formation inside the discharge ring.

4.4. Horizontal Vibration Measurements on the Turbine Guide Bearing

The pressure inside the turbine casing falls below the vapor pressure of the flowing water, and vibration occurs. This is brought on by poor design, frequent changes in

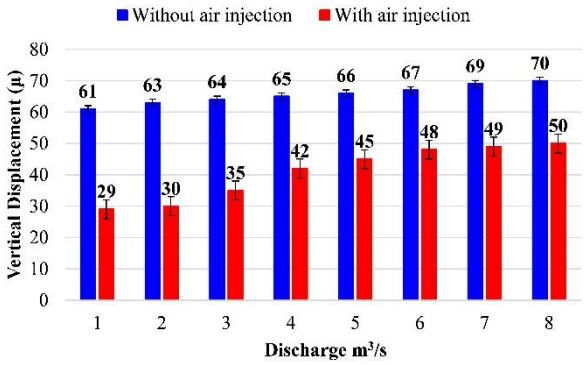

Fig. 8 Vertical displacement (µ) of discharge ring during air injection test

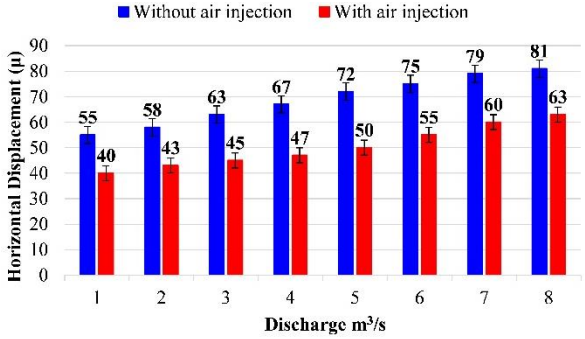

Fig. 9. Horizontal vibration measurements on the turbine guide bearing

operating conditions, and a turbine runner positioned at the tailrace level in the incorrect position. All three criteria mentioned are present in our experiments, which encourages cavitation inside the turbine casing. Hence, it is mandatory to stop the phenomenon of cavitation with pressurized air injection inside the turbine casing to eat away at the vacuum. Thus, Fig. 9 and the table below compare the horizontal vibration of the turbine guide bearing during the air injection test. Significant vibration level reductions are observed during air injection for discharges between 45 and 75 m^3/s, and perceptible vibration level reductions in the horizontal direction are seen for discharges beyond 75 m^3/s.

4.5. Measures of Noise Levels

Measurements of the discharge ring's noise levels taken during an air injection test are compared in Fig. 10. During air injection, the noise level is noticeably reduced for discharges more significantly than 75 m^3/s and drastically reduced for discharges between 45 and 75 m^3/s.

4.5.1. Uncertainty Analysis

To perform an uncertainty analysis, consideration of significant factors and uncertainties:

Horizontal and Vertical Displacement:

Sensor Accuracy: ±1 µ

Experimental Variability: ±2 µ

Data Processing and Analysis: ±1 µ

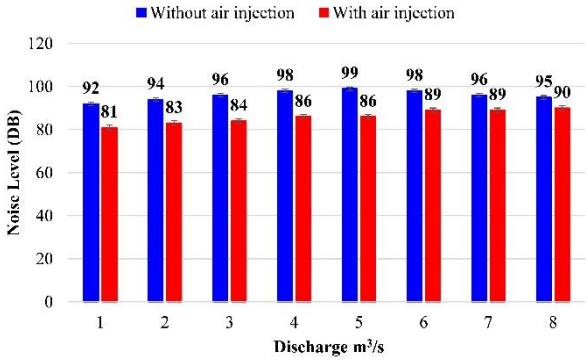

Fig. 10. Comparison of noise level measurement

$$\text{Combined standard uncertainty} = \sqrt{(Sensor\ accuracy)^2 + (Experimental\ variability)^2 + +(Data\ processing\ and\ analysis)^2}$$

$$= \sqrt{(1)^2 + (2^2) + (1^2)}$$

$$= \pm 2.44$$

Noise Levels:

Sound Level Meter Accuracy: ±1 dB

Experimental Variability: ±2 dB

Data Processing and Analysis: ±1 dB

Combined standard uncertainty: ± 2.44

Tables 4 and 5 illustrate that the measurements are reported as the mean value with an expanded uncertainty of k=2. As an illustration, the value "55 ± 2.44" indicates that the actual horizontal displacement at a discharge of 45 m^3/s is expected to fall within the range of 52.56 µ and 57.44 µ, with a confidence level of around 95%.

Table 4 Uncertainty for horizontal and vertical displacement

Discharge (m^3/s)	Horizontal Displacement (µ)	Vertical Displacement (µ)
45	55 ± 2.44	61 ± 2.44
55	58 ± 2.44	63 ± 2.44
75	63 ± 2.44	64 ± 2.44
95	67 ± 2.44	65 ± 2.44
125	72 ± 2.44	66 ± 2.44
185	75 ± 2.44	67 ± 2.44
235	79 ± 2.44	69 ± 2.44
275	81 ± 2.44	70 ± 2.44

Table 5 Uncertainty for Noise level

Discharge (m^3/s)	Noise Levels (dB)
45	92±2.44
55	94±2.44
75	96±2.44
95	98±2.44
125	99±2.44
185	98±2.44
235	96±2.44
275	95±2.44

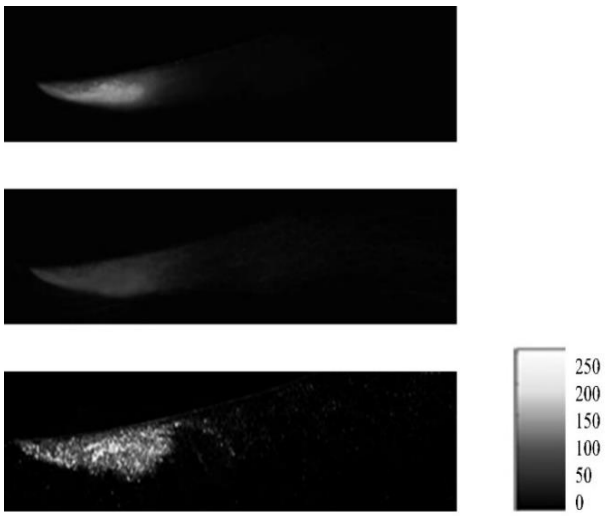

Fig. 11 The first hydrofoil, the top one, shows cavitation, the middle one spatially averages a grey level, and the bottom one shows the standard deviation of the grey level. The grey level's standard deviation is 2.27, the hydrofoil's working pressure is 0.15 bar, and its flow rate is 61.7 m³/h

Regarding noise levels, it is common practice to report measurements as the mean value and the expanded uncertainty (k=2). As an illustration, the value "92 ± 2.44" indicates that the actual noise level at a discharge of 45 m³/s is expected to fall within the range of 89.56 dB to 94.44 dB, with a confidence level of around 95%. This uncertainty analysis offers a thorough comprehension of the possible errors and variations linked to the measured horizontal and vertical displacements and noise levels, guaranteeing the accuracy and dependability of the reported values.

4.6. Cavitation Image Analysis

Analysis was performed on the time series of pictures acquired from the cavitation tunnel's high-speed visualization to identify specific traveling bubbles. First, we eliminated tiny, bright objects from the images while keeping associated cavitation and cavitation clouds. From these processed photos, we calculated the standard deviation and average grey level (Eg(i,j,t)). After separating the intensity range into intervals of 256 grey levels (8-bit camera picture depth), Eg(i,j,t) was generated by Kavurmaci et al. (2013). These levels range from white (intensity = 255), the highest possible value, to black (intensity = 0). From there, we averaged the grey level series inside the study area. This equation was used to estimate the standard.

$$S(i,j) = \sqrt{\frac{1}{T}\sum_{t=1}^{T}[E(i,j,t) - \big(Eg(i,j)\big)]^2} \ldots\ldots \quad (7)$$

This is where the cavitation structure's average void percentage is proportional to ⟨Eg (i,j)⟩, which stands for the temporal and spatially averaged grey level.

$$\langle Eg(i,j)\rangle = 1/T \sum^{T}_{(t=1)} [\![E(i,j,t)]\!] \cdots\cdots \quad \cdots (8)$$

The length and frequency of picture capture are used to define the time interval "t" in Equations (7) and (8).

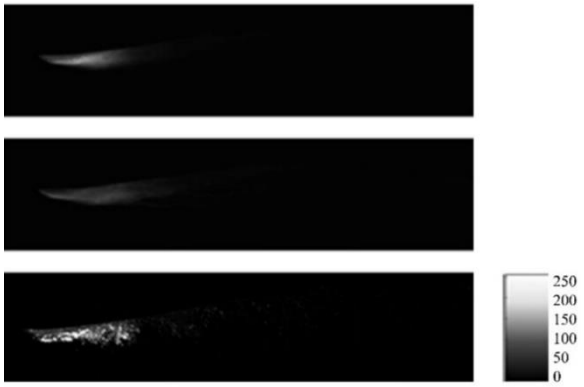

Fig. 12 One shows cavitation at the top, another shows a spatially averaged grey level in the center, and the third shows the standard deviation of the grey level at the bottom. A pressure of 0.15 bar, a flow rate of 61.7 m³/h, and a standard deviation value of 2.27 are the working conditions of this modified hydrofoil

The image analysis for the current hydrofoil is shown in Fig. 11, with the following parameters: pressure (p) = 0.15 bar, volumetric flow rate (Q) = 61.7 m³/h, cavitation number (σ) = 2.27. Figure 9 shows the analysis for the improved hydrofoil under the same circumstances Celebioglu et al. (2024). The anticipated cavitation length for the redesigned hydrofoil was 11.27 mm, and for the conventional hydrofoil, it was 22.74 mm at the chosen operating conditions. Regression cavitation length modeling used this approach to estimate cavitation length, which was uniformly applied across all operating locations for both hydrofoils. Figures 11 and 12 illustrate the cavitation of the original and modified hydrofoil.

4.6.1. Cavitation Number σ Influences Cavitation

Figures 13–16 show the two hydrofoils when the cavitation number (σ) is reduced, allowing for a visual comparison and study. We chose cavitation numbers in decreasing order to highlight disparities in the incidence of cavitation structures. Selecting photos showing the hydrofoil suction side in their most usual settings is the main goal for each cavitation number (σ) picked. The severity and the frequency of cavitation structures are enhanced when the cavitation number is decreased. This discovery shows the importance of form adjustment in enabling cavitation on hydrofoils. Cavitation phenomena are less severe in a modified hydrofoil than in an unmodified hydrofoil Zharkovskiy et al. (2023). The main visible areas are the leading edge and the whole suction side of the hydrofoil. Understanding the impact of cavitation on hydrofoil performance is greatly enhanced by this research, which also highlights the need to optimize the shape to reduce cavitation-related problems Li et al. (2021).

With an emphasis on relevant cavitation intensities, Figures 13–16 provide data acquired within specific cavitation number ranges that are possible in our cavitation tunnel. Cavitation begins on the redesigned hydrofoil at about σ = 3.65, according to the data shown in Figure 13, when the absolute pressure is pubs = 0.65 bar (Wang et al., 2021; Li et al., 2022). At first, cavitation,

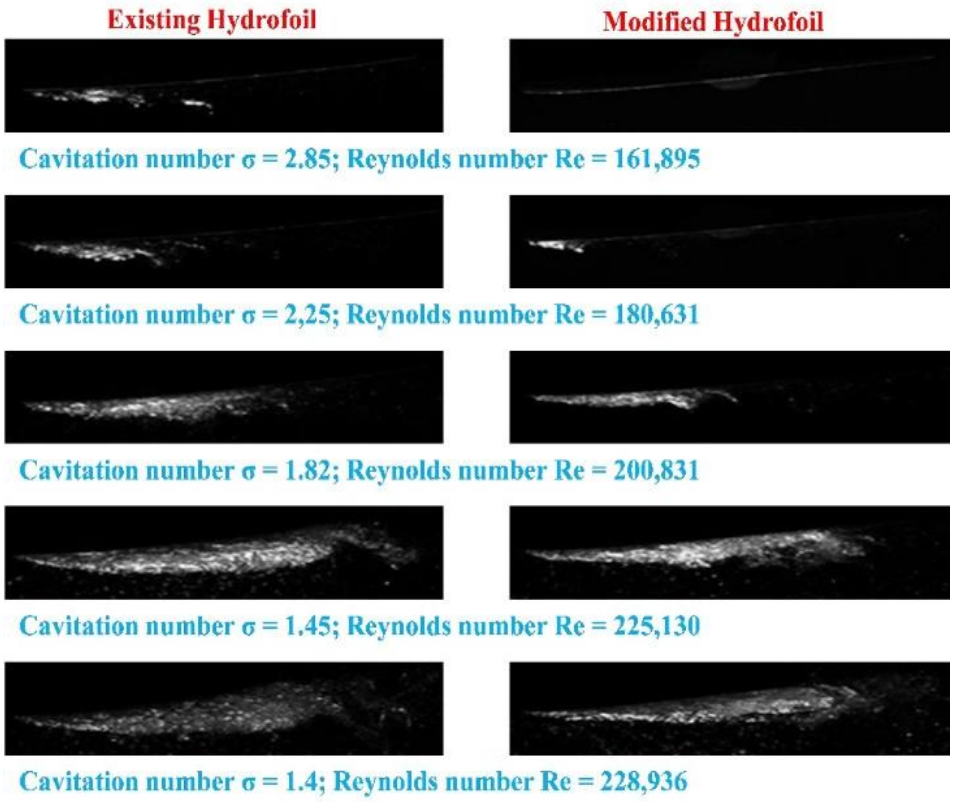

Fig. 13 Cavitation structures at P_{abs}=0.15 bar

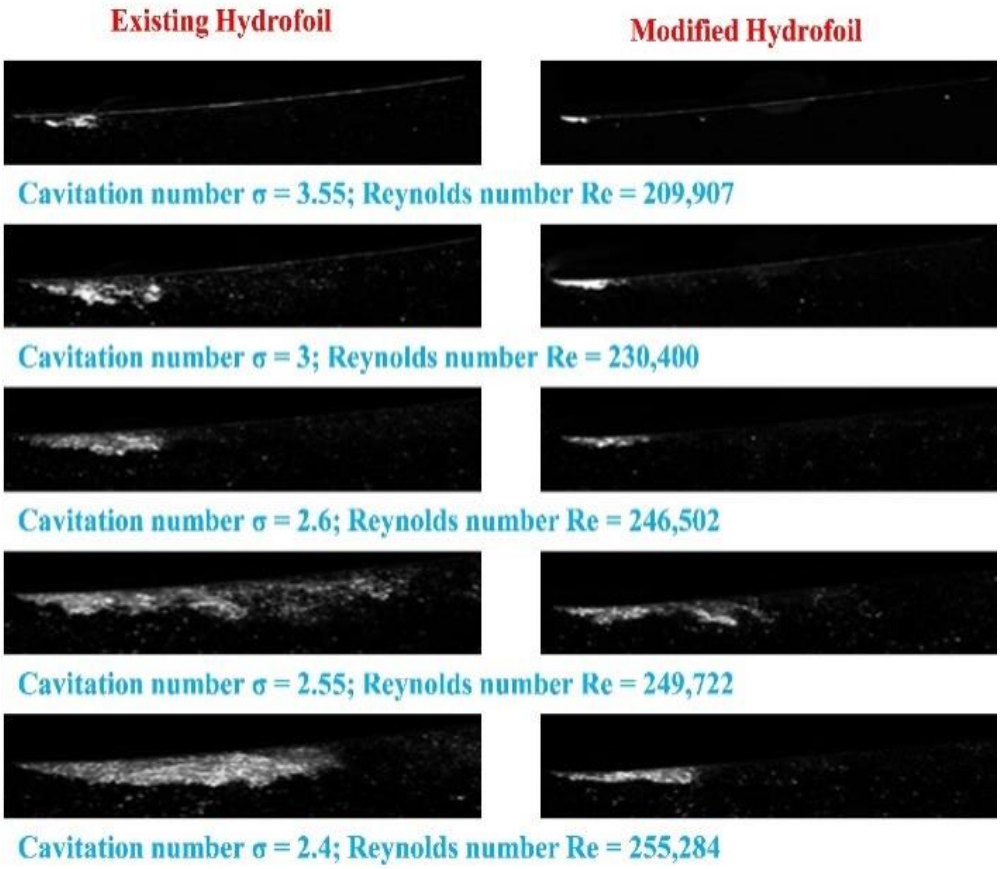

Fig. 14 Cavitation structures atP_{abs}=0.30 bar

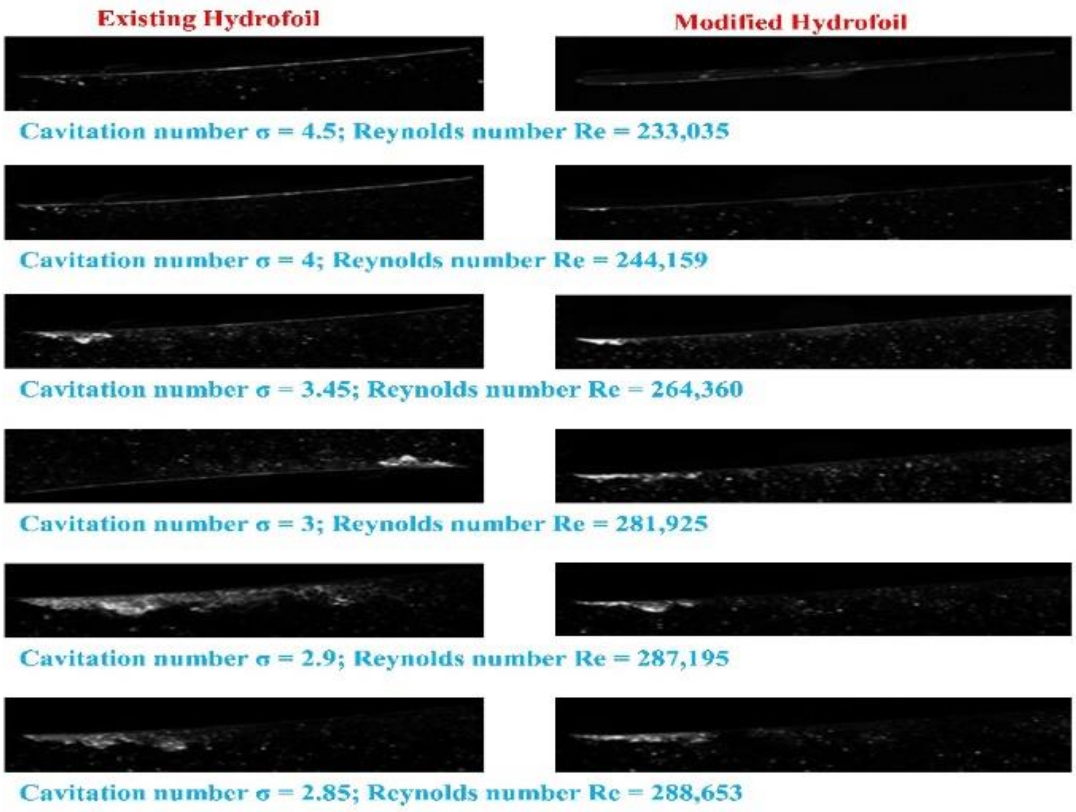

Fig. 15 Cavitation structures at P_{abs}=0.45 bar

which is linked to the leading edge, develops. The shedding of cavitation clouds occurs at quasi-periodic intervals when the cavitation number drops to about σ = 3.1 and the cavitation intensity rises. Conversely, cavitation happens on the first hydrofoil with more significant cavitation numbers, approximately around σ = 4.45. Some cloud shedding due to cavitation is seen at i = 3.65, affecting more than two-thirds of the hydrofoil at F = 3.1. The cavitation length on the modified hydrofoil is only one-third of the hydrofoil length at F = 3.1, which is worth noting. Dissimilarities in the curvature and geometry of the leading edge, which influence the separation of flows and cause cavitation to initiate at low absolute pressure and high velocity, are probably to blame for this disparity. Cavitation begins on the modified hydrofoil at about σ = 3.45 when the total pressure is P_{abs} = 0.45 bar, as shown in Fig. 14. Like in the first instance, attached cavitation begins behind the leading edge. Cavitation cloud shedding becomes apparent when σ = 3. Cavitation starts sooner and is more severe on the original hydrofoil, starting at about σ = 4.5 and covering almost the whole hydrofoil by τ = 3.

Cavitation development around σ = 3.55 is seen in Fig. 15, with associated cavitation developing as incipient cavitation, while the absolute pressure is p_{ubs} = 0.30 bar. Roughly half of the hydrofoil's length is covered by attached cavitation in the modified hydrofoil, which occurs at around σ = 3 (Zhang et al. 2021; François, L. 2012). Likewise, the first hydrofoil encounters cavitation onset at about σ = 3.55, but to a lesser extent. It should be noted that the original hydrofoil experiences more widespread cavitation at σ = 3.0, accompanied by an enormous cavitation cloud. A dense cavitation cloud covers the original hydrofoil below σ = 2.6. At an absolute pressure of 0.15 bar, Fig. 16 shows that the redesigned hydrofoil does not experience cavitation at about σ = 2.85. However, at σ = 2.25, cavitation clouds cover up to one-third of the hydrofoil's length Guo et al. (2018). The cavitation cloud becomes more intense at σ = 1.82, and both hydrofoils are completely engulfed in super cavitation below σ = 1.45. These results point to the redesigned hydrofoil having desirable cavitation properties, which might lead to better performance in cavitation-prone settings like bulb turbines Arunraj et al. (2023). The study examines the effectiveness of air injection in reducing vibration and noise levels in bulb turbines. Injecting air into the turbine helps to reduce cavitation, resulting in a notable decrease in vibration and noise levels. As an illustration, the introduction of air injection when operating at 2 MW results in a decrease in vibration levels. Specifically, the average vertical vibration level is reduced from 245 μ to 168 μ, while the horizontal vibration level is reduced from 66 μ to 43 μ, as compared to operating without air injection. In a shutdown scenario with air injection, the noise levels decrease significantly. Vertically, the average drops from 121 dB to 99 dB, while horizontally it goes from 96 dB to 84 dB. The analysis of cavitation reveals that the performance of modified hydrofoils with air injection is enhanced, as the length of cavitation consistently decreases in comparison to the original hydrofoil. Flow analysis provides additional evidence supporting the advantages of air injection, demonstrating enhanced flow stability and decreased cavitation areas. Incorporating air injection and hydrofoil modifications improves turbine performance, resulting in a significant reduction in noise

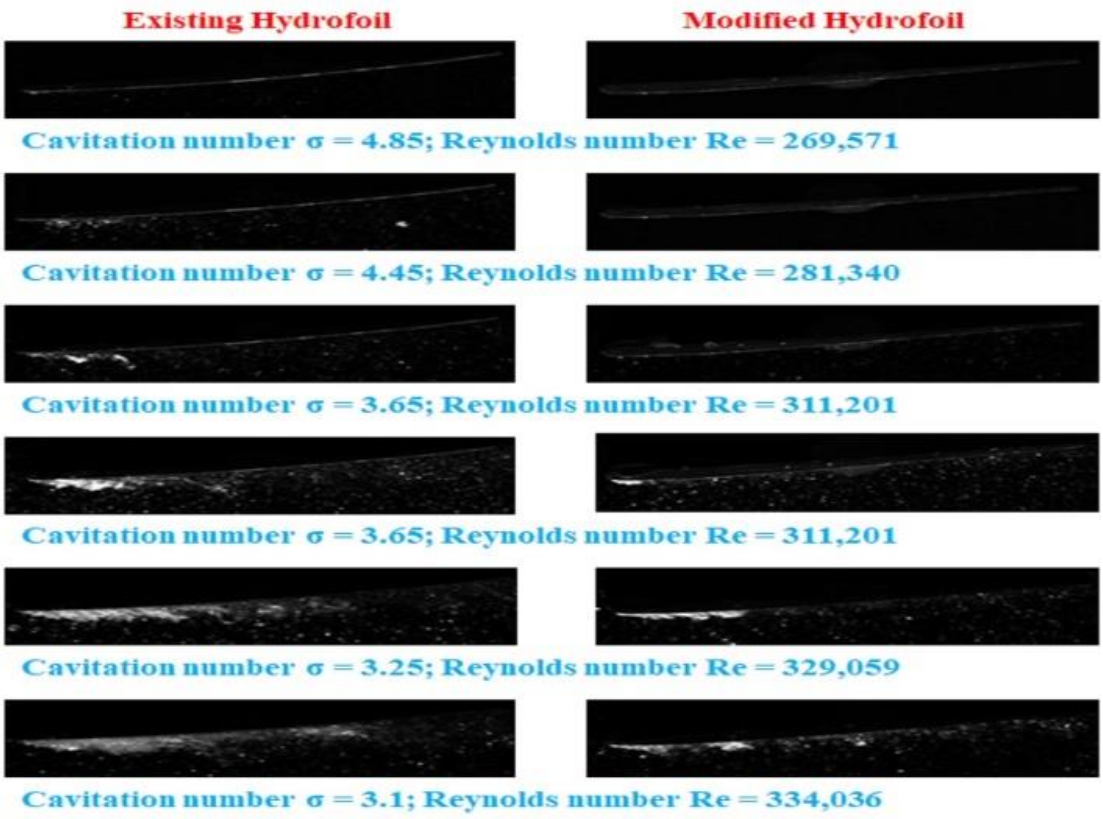

Fig. 16 Cavitation and Reynolds Numbers at P_{abs}=0.65 bar

Fig. 17 Mesh file of the Hydrofoil design

levels by 10 dB on average and a 30% decrease in vibrations during shutdown. This underscores the significance of employing innovative methods in the pursuit of sustainable energy generation.

4.6.2. Velocity and Pressure Distribution

Figure 17 shows the meshing of the hydrofoil section. Figure 18, depicted in Computational Fluid Dynamics (CFD), presents various aspects of fluid flow around a hydro turbine. Each figure (a, b, c, and d) provides distinct insights and numerical comparisons. Figure 18 (a) depicts a color map illustrating the fluid velocity magnitude surrounding the turbine. The values range from 0 m/s (dark blue) in close proximity to the turbine's boundaries to 108.83 m/s (red) in areas of significant fluid motion. Figure 18 (b) displays contour lines on the velocity magnitude map, indicating areas of continuous velocity and exposing significant velocity gradients in close proximity to the turbine blades.

The recorded values range from 21.706 m/s to 87.062 m/s. Figure 18 (c) illustrates streamlines that illustrate the direction and magnitude of fluid flow around the turbine, suggesting the possibility of vortex formation in its aftermath. The velocities observed in Fig. 18 (c) are comparable to those depicted in Fig. 18 (a). In Fig. 18 (d), the tangential velocity component is depicted, showcasing rotational motion around the turbine blades and varying rotational directions. The scale ranges from -40.004 m/s (dark blue) to 102.19 m/s (dark red). This study offers a comprehensive analysis of the fluid-structure interaction in the hydro turbine by comparing various visualization techniques. It focuses on variations in flow acceleration, deceleration, separation, and vortex shedding. Figure 19 employs Computational Fluid Dynamics (CFD) to depict the pressure distribution surrounding a hydro turbine. Figure 19 (a) displays a pressure contour map illustrating a pressure range of -1623.2 Pa (dark blue) to 8254.8 Pa (red), with lines superimposed. The diagram displays contrasting pressure gradients around the turbine blades, with high pressure on the upstream side (red) and low pressure on the downstream side (dark blue). The contour lines are closely spaced, indicating steep pressure gradients. In Fig. 19 (b), a smooth color map without contour lines illustrates the pressure distribution, highlighting the significant pressure disparity. The upstream side exhibits high pressure (red to orange) while the downstream side displays low pressure (blue to dark blue). Figure 19 (c) exclusively exhibits contour lines, emphasizing intricate pressure gradients and discerning regions of elevated pressure (red lines) and diminished

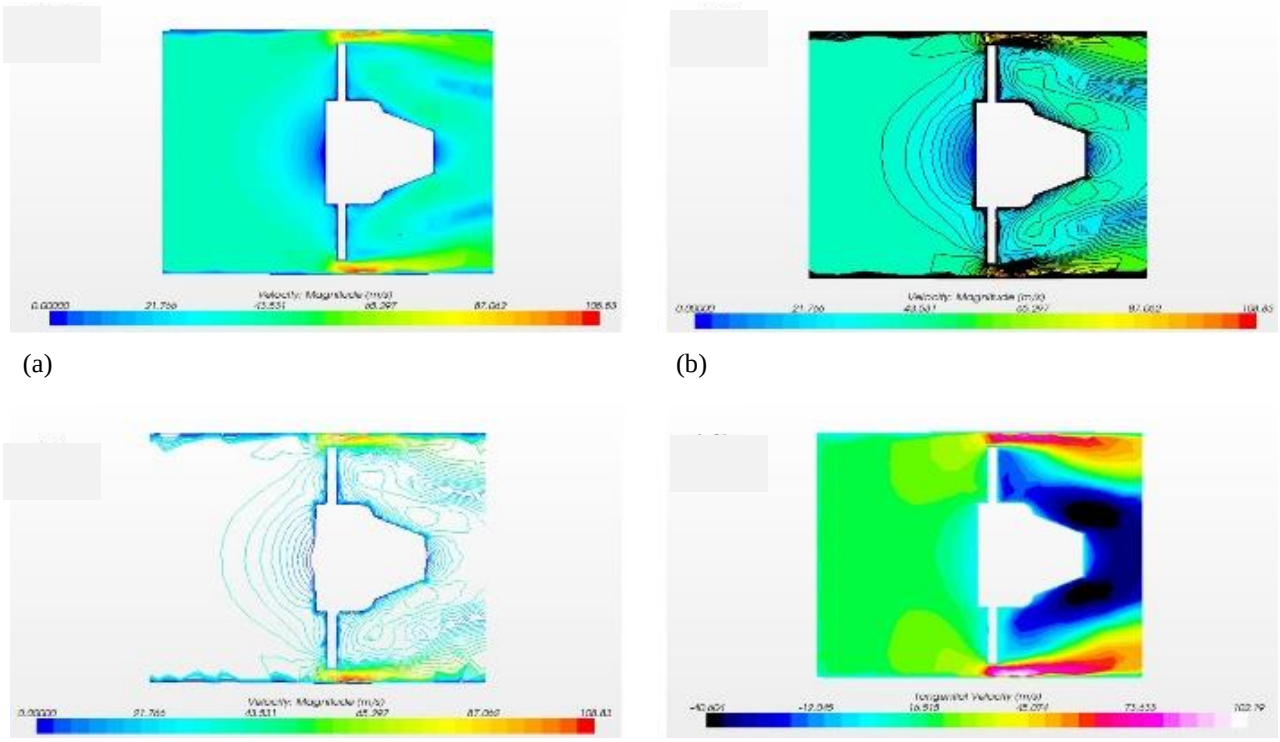

(a) (b)

(c) (d)

Fig. 18 Velocity contour

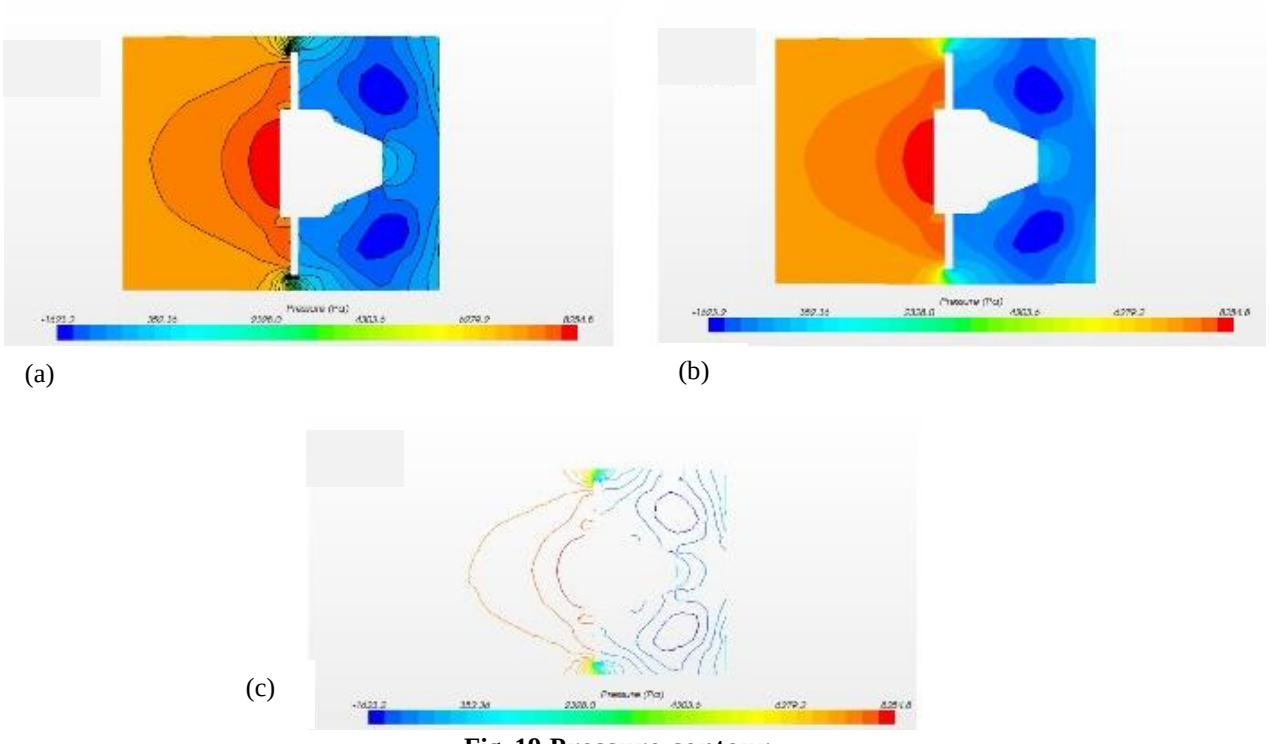

(a) (b)

(c)

Fig. 19 Pressure contour

pressure (blue lines). Figures 19 illustrate the notable pressure fluctuations resulting from the turbine. The maximum pressure upstream reaches 8254.8 Pa, while it decreases to -1623.2 Pa downstream. These figures are essential for comprehending the turbine's influence on fluid flow and operational efficiency. Velocity vector plots are valuable tools for visualizing the direction and magnitude of flow within a turbine. These plots allow us to observe how the flow moves and changes when air is introduced. When operating conditions are set at P_{abs} = 0.15 bar and Q = 61.7 m^3/h, the velocity vectors reveal the flow pattern around the hydrofoil. Notably, areas of high velocity are concentrated near the leading edge, while lower velocities can be observed downstream. We can identify cavitation regions by analyzing disrupted flow patterns or low-velocity areas. The velocity vectors for the

modified hydrofoil demonstrate the altered flow pattern compared to the original design, showcasing changes in velocity distribution due to hydrofoil modifications. These changes result in improved flow stability and reduced cavitation areas compared to the original hydrofoil.

On the other hand, Streamline plots provide a visual representation of the flow paths within the turbine. They offer insights into how fluid particles move through the system, allowing us to understand flow behavior. When examining the streamlined plots around the hydrofoil, we can identify areas of separation and recirculation. Disrupted or irregular streamlines may indicate cavitation regions. We can observe how cavitation affects the flow pattern by analyzing the streamline plots. Changes in flow paths compared to the original design can be observed for the modified hydrofoil. These changes result in improved flow stability and reduced separation zones.

Additionally, cavitation regions may be minimized or eliminated, leading to a more uniform flow distribution. To gain a comprehensive understanding of flow behavior and the impact of hydrofoil modification and air injection, it is beneficial to present both velocity vector plots and streamline plots side by side. This allows for a holistic analysis of the changes in flow behavior with and without air injection. The visualizations highlight the effectiveness of the modified hydrofoil and air injection in achieving improved flow stability, reduced cavitation areas, and more uniform flow distribution.

4.6.3. Cost Estimation Analysis

$$E_{saving} = E_{before} \times \frac{Reduction\%}{100} \ldots\ldots\ldots \quad (9)$$

$$\text{Payback period} = \frac{Cost}{Energy\ Cost\ Savings} \ldots\ldots \quad (10)$$

This study aims to determine the energy savings and payback period associated with the implementation of mitigation measures on a bulb turbine. The equations 9 and 10 used to determine the Energy saving and payback period. The turbine's pre-mitigated annual energy consumption is 1,500 megawatt-hours (MWh). A 10% decrease in energy consumption results in annual energy savings of 150 megawatt-hours (MWh). The implementation of these measures incurs a cost of $150,000. Given the average electricity cost in India of $50 per MWh, the estimated annual energy cost savings amount to $7,500. The mitigation measures have a payback period of 20 years, indicating that the initial investment will be recouped through energy savings within this timeframe.

5. CONCLUSION

Vibration and noise levels are vertically gauged at the discharge ring's top. It should be noted that vibration and noise levels are measured in various operating modes. Because the runner vane closes suddenly and quickly at 2 MW, the peak values for vibration and noise levels are obtained at the shutdown of the machine generating 2 MW rather than the shutdown of the machine generating 5 MW. As can be seen in the table, at 2 W, the maximum vibration level was 77 microns, and at 5 MW, the maximum noise level was 73 microns and 100 dB. In bulb turbines, air injection has been tried effectively to reduce cavitation erosion and has been proven to be quite effective. During these air injection studies, an average noise reduction of 10 dB and a 30% vibration suppression during shutdown were noted.

When operating at 2 MW with air injection, vibration levels are reduced from 245 μ to 168 μ vertically and rom 66 μ to 43 μ horizontally. Similarly, noise levels drop from 121 dB to 99 dB vertically and from 96 dB to 84 dB horizontally during shutdown.

In this research, it was exposed that applying compressed air to low-pressure areas within the discharging decreased cavity collapses and the harmful consequences of cavitation. The vacuum in the cavitation zones is broken by the injection of compressed air, which raises the pressure and eliminates the cavitation. Massive bubbles are formed by injecting air when the air exerts an enormous cushioning effect that the liquid cannot detect as the bubble contracts. The bubbles are compressed in the high-pressure region downstream, but they are kept from collapsing. The vibration was reduced by 50%, and the noise level at the lower guide vane apertures increased by 15 dB from 30% to 50% when compressed air was introduced into the bulb turbine's runner vane moving area.

The effect of hydrofoil form on cavitation was the intended focus of the investigation. Original and modified hydrofoils were taken from runner blades with a 95% radius and fine-tuned with an emphasis on the leading edge, thickness, and curvature. Efforts were made to stabilize the flow towards the trailing edge and avoid flow separation. The two hydrofoils were subjected to identical energy testing in a bulb turbine.

Air injection into the turbine has been found to impact reducing noise levels during operation substantially. For discharge rates exceeding 75 m^3/s, a discernible decrease in noise is observed, with a significant reduction occurring for discharges ranging from 45 to 75 m^3/s. The analysis of cavitation indicates that the modified hydrofoil demonstrates reduced cavitation compared to the original hydrofoil at different cavitation numbers. The cavitation length on the modified hydrofoil consistently decreased, suggesting enhanced performance and reduced. Reducing the cavitation number leads to an increase in both the severity and frequency of cavitation structures. Nevertheless, the impact of these phenomena is mitigated in the modified hydrofoil compared to the original design.

The velocity vector plots indicate a high velocity concentration near the hydrofoil's leading edge while the velocities decrease downstream. The modified hydrofoil showcases adjusted flow patterns, enhancing flow stability and decreased cavitation areas compared to the original design. The plots demonstrate the reduction of separation zones and the elimination or minimization of cavitation regions for the hydrofoil modified with air injection.

The cavitation length on the modified hydrofoil is significantly shorter compared to the original hydrofoil in different scenarios. When air injection is used, the noise levels during operation are reduced by an average of 10

dB, resulting in a quieter turbine operation. Air injection effectively reduces vibration levels, which in turn enhances turbine performance and increases its lifespan.

It is ultimately, integrating air injection and hydrofoil modifications results in improved turbine performance. This is achieved through the reduction of cavitation-related problems, the mitigation of noise and vibration, and the enhancement of flow stability. The significance of these findings lies in the need for creative approaches to address cavitation and enhance turbine performance to achieve sustainable energy generation.

CONFLICT OF INTEREST

On behalf of all authors, the corresponding author states that there is no conflict of interest.

AUTHORS CONTRIBUTION

S. Praveen: Conceptualization, Draft writing, Software. **S. Marimuthu:** Methodology, Writing – review & editing. **Bader Alqahtani:** Investigation, Methodology and Paper writing. **G. Bharathiraja:** Methodology, Supervision. **G. Gokilakrishnan:** Conceptualization, Data curation, Resources, Methodology, Validation, Formal Analysis, Data curation, Supervision, Writing – review & editing.

REFERENCES

Al-Obaidi, A. R. (2019). Investigation of effect of pump rotational speed on performance and detection of cavitation within a centrifugal pump using vibration analysis. *Heliyon*, *5*(6), e01910. https://doi.org/10.1016/j.heliyon.2019.e01910

Al-Obaidi, A. R. (2023a). Effect of different guide vane configurations on flow field investigation and performances of an axial pump based on CFD analysis and vibration investigation. *Experimental Techniques*, *48*(1), 69–88. https://doi.org/10.1007/s40799-023-00641-5

Al-Obaidi, A. R. (2023b). Experimental diagnostic of cavitation flow in the centrifugal pump under various impeller speeds based on acoustic analysis method. (2023). *Archives of Acoustics*. https://doi.org/10.24425/aoa.2023.145234

Al-Obaidi, A. R. (2024). Evaluation and investigation of hydraulic performance characteristics in an axial pump based on CFD and acoustic analysis. *Processes*, *12*(1), 129. https://doi.org/10.3390/pr12010129

Al-Obaidi, A. R., & Alhamid, J. (2023). Investigation of the main flow characteristics mechanism and flow dynamics within an axial flow pump based on different transient load conditions. *Iranian Journal of Science and Technology, Transactions of Mechanical Engineering*, *47*(4), 1397–1415. https://doi.org/10.1007/s40997-022-00586-x

Al-Obaidi, A., Khalaf, H., & Alhamid, J. (2023a, November 24). *Investigation of the influence of varying operation configurations on flow behaviors characteristics and hydraulic axial-flow pump performance.* Proceedings of the 4th International Conference on Science Education in the Industrial Revolution 4.0, ICONSEIR 2022, Medan, Indonesia. https://doi.org/10.4108/eai.24-11-2022.2332719

Al-Obaidi, A., Khalaf, H., & Alhamid, J. (2023b, 24 November 24). *Investigation on the characteristics of internal flow within three-dimensional axial pump based on different flow conditions.* Proceedings of the 4th International Conference on Science Education in the Industrial Revolution 4.0, ICONSEIR 2022, Medan, Indonesia. https://doi.org/10.4108/eai.24-11-2022.2332720

Arunraj, P. V., Vasanthkumar, P., Senthilkumar, N., & Dhandapani, K. (2023). *Fabrication and characterization of ceramic foam material for vibration reduction.* AIP Conference Proceedings. https://doi.org/10.1063/5.0119700

Brennen, C. E., Meissner, C., Lo, E. Y., & Hoffman, G. S. (1982). Scale effects in the dynamic transfer functions for cavitating inducers. *Journal of Fluids Engineering*, *104*(4), 428–433. https://doi.org/10.1115/1.3241875

Candel, I., Bunea, F., Dunca, G., Bucur, D. M., Ioana, C., Reeb, B., & Ciocan, G. D. (2014). *Detection of cavitation vortex in hydraulic turbines using acoustic techniques.* IOP Conference Series: Earth and Environmental Science. https://doi.org/10.1088/1755-1315/22/5/052007

Celebioglu, K., Altintas, B., Aradag, S., & Tascioglu, Y. (2017). Numerical research of cavitation on Francis turbine runners. *International Journal of Hydrogen Energy*, *42*(28), 17771–17781. https://doi.org/10.1016/j.ijhydene.2017.03.180

Celebioglu, K., Ayli, E., Cetinturk, H., Tascioglu, Y., & Aradag, S. (2024). Exploring the potential of artificial intelligence tools in enhancing the performance of an inline pipe turbine. *Proceedings of the Institution of Mechanical Engineers, Part E: Journal of Process Mechanical Engineering.* https://doi.org/10.1177/09544089231224324

Cervone, A., Tsujimoto, Y., & Kawata, Y. (2009). Evaluation of the dynamic transfer matrix of cavitating inducers by means of a simplified "lumped-parameter" model. *Journal of Fluids Engineering*, *131*(4). https://doi.org/10.1115/1.3089535

Cheng, H., Ji, B., Long, X., Huai, W., & Farhat, M. (2021a). A review of cavitation in tip-leakage flow and its control. *Journal of Hydrodynamics*, *33*(2), 226–242. https://doi.org/10.1007/s42241-021-0022-z

Cheng, H., Long, X., Ji, B., Peng, X., & Farhat, M. (2021b). A new Euler-Lagrangian cavitation model for tip-vortex cavitation with the effect of non-condensable gas. *International Journal of Multiphase Flow*, *134*, 103441. https://doi.org/10.1016/j.ijmultiphaseflow.2020.103441

Cherny, S., Chirkov, D., Bannikov, D., Lapin, V.,

Skorospelov, V., Eshkunova, I., & Avdushenko, A. (2010). *3D numerical simulation of transient processes in hydraulic turbines.* IOP Conference Series: Earth and Environmental Science . https://doi.org/10.1088/1755-1315/12/1/012071

Dhinakarraj, C. K., Senthilkumar, N., Badri, M. A., & Anbuchezhiyan, G. (2020). Vibration and damping behavior of Si3N4 reinforced magnesium alloy composite for structural applications. *Journal of New Materials for Electrochemical Systems, 23*(3), 182–189. https://doi.org/10.14447/jnmes.v23i3.a05

Dönmez, A. H., Yumurtacı, Z., & Kavurmacıoğlu, L. (2023). Influence of inlet vane and wrap angles on cavitation behavior of a centrifugal pump. *Journal of Applied Fluid Mechanics, 16*(3), 519-531. https://doi.org/10.47176/jafm.16.03.1342

Feng, J., Benra, F. K., & Dohmen, H. J. (2010). Application of different turbulence models in unsteady flow simulations of a radial diffuser pump. *Forschung Im Ingenieurwesen, 74*(3), 123–133. https://doi.org/10.1007/s10010-010-0121-4

François, L. (2012). *Vibratory detection system of cavitation erosion: historic and algorithm validation*. Proceedings of the 8th International Symposium on Cavitation. https://doi.org/10.3850/978-981-07-2826-7_150

Gao, B., Guo, P., Zhang, N., Li, Z., & Yang, M. (2017). Experimental investigation on cavitating flow induced vibration characteristics of a low specific speed centrifugal pump. *Shock and Vibration, 2017*, 1–12. https://doi.org/10.1155/2017/6568930

Grist, E. (2023). *Cavitation — An Unacceptable Phenomenon. Cavitation And The Centrifugal Pump*, 1–10. https://doi.org/10.1201/9781315138923-1

Guo, Q., Zhou, L., Wang, Z., Liu, M., & Cheng, H. (2018). Numerical simulation for the tip leakage vortex cavitation. *Ocean Engineering, 151*, 71–81. https://doi.org/10.1016/j.oceaneng.2017.12.057

Hu, Q. X., Yang, Y., & Shi, W. D. (2020). Cavitation simulation of centrifugal pump with different inlet attack angles. *International Journal of Simulation Modelling, 19*(2), 279–290. https://doi.org/10.2507/ijsimm19-2-516

Huang, B., Ducoin, A., & Lu Young, Y. (2012). *Evaluation of cavitation models for prediction of transient cavitating flows around a stationary and a pitching hydrofoil.* Proceedings of the 8th International Symposium on Cavitation. https://doi.org/10.3850/978-981-07-2826-7_284

Jin, J., Fan, Y., Han, W., & Hu, J. (2012). Design and analysis on hydraulic model of the ultra -low specific-speed centrifugal pump. *Procedia Engineering, 31*, 110–114. https://doi.org/10.1016/j.proeng.2012.01.999

Kavurmaci, B., Akin, H., Ayli, E., Celebioglu, K., & Aradag, S. (2013). *Design of an experimental test stand for francis type hydraulic turbines.* 4th International Conference on Power Engineering, Energy and Electrical Drives. https://doi.org/10.1109/powereng.2013.6635725

Kral, L. D. (1998). Recent experience with different turbulence models applied to the calculation of flow over aircraft components. *Progress in Aerospace Sciences, 34*(7–8), 481–541. https://doi.org/10.1016/s0376-0421(98)00009-8

Li, R., Wen, Q., Tan, W., & Zhang, Y. (2018). Adaptive weighting impact angle optimal guidance law considering seeker's FOV angle constraints. *Journal of Systems Engineering and Electronics, 29*(1), 142–151. https://doi.org/10.21629/jsee.2018.01.14

Li, W., Li, S., Ji, L., Li, E., Shi, W., Agarwal, R., & Awais, M. (2022). Effect of inlet elbow on rotation stall in waterjet propulsion pump. *Fundamental Research.* https://doi.org/10.1016/j.fmre.2022.05.029

Li, W., Li, S., Ji, L., Zhao, X., Shi, W., Agarwal, R. K., Awais, M., & Yang, Y. (2021). A study on the cavitation and pressure pulsation characteristics in the impeller of an LNG submerged pump. *Machines, 10*(1), 14. https://doi.org/10.3390/machines10010014

Limbach, P., & Skoda, R. (2017). Numerical and experimental analysis of cavitating flow in a low specific speed centrifugal pump with different surface roughness. *Journal of Fluids Engineering, 139*(10). https://doi.org/10.1115/1.4036673

Lin, P., Yang, T., Xu, W., & Zhu, Z. (2022). Influence of different offset angles of inlet guide vanes on flow characteristics of centrifugal pump. *Frontiers in Energy Research, 10*. https://doi.org/10.3389/fenrg.2022.818244

Lindsay, R. B. (1970). On the pressure developed in a liquid during the collapse of a spherical cavity (1917). Men of Physics: Lord Rayleigh–The Man and His Work, 221–226. https://doi.org/10.1016/b978-0-08-006821-3.50028-3

Nohmi, M., Ochiai, N., Iga, Y., & Ikohagi, T. (2010). *A detailed observation of hydrofoil cavitation and a proposal for improving cavitation model.* ASME 2010 3rd Joint US-European Fluids Engineering Summer Meeting: Volume 2, Fora. https://doi.org/10.1115/fedsm-icnmm2010-30435

Plesset, M. S., & Prosperetti, A. (1977). Bubble dynamics and cavitation. *Annual Review of Fluid Mechanics, 9*(1), 145–185. https://doi.org/10.1146/annurev.fl.09.010177.001045

Sun, H., Xiao, R., Wang, F., Xiao, Y., & Liu, W. (2014). Analysis of the pump-turbine S characteristics using the detached eddy simulation method. *Chinese Journal of Mechanical Engineering, 28*(1), 115–122. https://doi.org/10.3901/cjme.2014.1021.159

Tanaka, T., & Tsukamoto, H. (1999). Transient behavior of a cavitating centrifugal pump at rapid change in operating conditions—Part 1: Transient phenomena at opening/closure of discharge valve. *Journal of Fluids Engineering, 121*(4), 841–849.

https://doi.org/10.1115/1.2823545

Wang, C., Zhang, Y. X., Zhang, J. Y., Li, Z. W., & Xu, A. (2019). *Comparative research on various turbulence closure models for unsteady cavitation flows in the ultra-low specific speed centrifugal pump.* IOP Conference Series: Earth and Environmental Science, 240, 062038. https://doi.org/10.1088/1755-1315/240/6/062038

Wang, G., & Ostoja-Starzewski, M. (2007). Large eddy simulation of a sheet/cloud cavitation on a NACA0015 hydrofoil. *Applied Mathematical Modelling, 31*(3), 417–447. https://doi.org/10.1016/j.apm.2005.11.019

Wang, G., Yang, Y., Wang, C., Shi, W., Li, W., & Pan, B. (2021). Effect of nozzle outlet shape on cavitation behavior of submerged high-pressure jet. *Machines, 10*(1), 4. https://doi.org/10.3390/machines10010004

Zhang, D., Liu, Y., Kang, J., Zhang, Y., & Meng, F. (2022). The effect of discharge areas on the operational performance of a liquid-ring vacuum pump: Numerical simulation and experimental verification. *Vacuum, 206*, 111425. https://doi.org/10.1016/j.vacuum.2022.111425

Zhang, H., Meng, F., Zheng, Y., & Li, Y. (2021). The cavitation-induced pressure fluctuations in a mixed-flow pump under impeller inflow distortion. *Machines, 9*(12), 326. https://doi.org/10.3390/machines9120326

Zhang, J., Li, G., Mao, J., Yuan, S., Qu, Y., & Jia, J. (2019). Numerical investigation of the effects of splitter blade deflection on the pressure pulsation in a low specific speed centrifugal pump. *Proceedings of the Institution of Mechanical Engineers, Part A: Journal of Power and Energy, 234*(4), 420–432. https://doi.org/10.1177/0957650919867176

Zhang, Y. L., Yuan, S. Q., Zhang, J. F., Feng, Y. N., & Lu, J. X. (2014). *Numerical investigation of the effects of splitter blades on the cavitation performance of a centrifugal pump.* IOP Conference Series: Earth and Environmental Science. https://doi.org/10.1088/1755-1315/22/5/052003

Zharkovskiy, A. A., Schur, V. A., & Mohammad, O. (2023). Prediction of energy and cavitation characteristics of high specific speed Francis hydraulic turbines. *Izvestiya MGTU MAMI, 16*(3), 225–234. https://doi.org/10.17816/2074-0530-105208

Zhou, P. J., Wang, F. J., & Yang, M. (2012). *Internal flow numerical simulation of double-suction centrifugal pump using DES model.* IOP Conference Series: Earth and Environmental Science. https://doi.org/10.1088/1755-1315/15/3/032051

Zhu, Z. (2002). Experimental study on high-speed centrifugal pumps with different impellers. *Chinese Journal of Mechanical Engineering (English Edition), 15*(04), 372. https://doi.org/10.3901/cjme.2002.04.372